



HAL
open science

Carbon Nanofibers enhance the Fracture toughness and Fatigue Performance of a Structural Epoxy system

Daniel R. Bortz, César Merino, Ignacio Martin-Gullon

► **To cite this version:**

Daniel R. Bortz, César Merino, Ignacio Martin-Gullon. Carbon Nanofibers enhance the Fracture toughness and Fatigue Performance of a Structural Epoxy system. *Composites Science and Technology*, 2010, 71 (1), pp.31. 10.1016/j.compscitech.2010.09.015 . hal-00702320

HAL Id: hal-00702320

<https://hal.science/hal-00702320>

Submitted on 30 May 2012

HAL is a multi-disciplinary open access archive for the deposit and dissemination of scientific research documents, whether they are published or not. The documents may come from teaching and research institutions in France or abroad, or from public or private research centers.

L'archive ouverte pluridisciplinaire **HAL**, est destinée au dépôt et à la diffusion de documents scientifiques de niveau recherche, publiés ou non, émanant des établissements d'enseignement et de recherche français ou étrangers, des laboratoires publics ou privés.

Accepted Manuscript

Carbon Nanofibers enhance the Fracture toughness and Fatigue Performance of a Structural Epoxy system

Daniel R. Bortz, César Merino, Ignacio Martin-Gullon

PII: S0266-3538(10)00372-6
DOI: [10.1016/j.compscitech.2010.09.015](https://doi.org/10.1016/j.compscitech.2010.09.015)
Reference: CSTE 4818

To appear in: *Composites Science and Technology*

Received Date: 28 June 2010
Revised Date: 22 September 2010
Accepted Date: 25 September 2010

Please cite this article as: Bortz, D.R., Merino, C., Martin-Gullon, I., Carbon Nanofibers enhance the Fracture toughness and Fatigue Performance of a Structural Epoxy system, *Composites Science and Technology* (2010), doi: [10.1016/j.compscitech.2010.09.015](https://doi.org/10.1016/j.compscitech.2010.09.015)

This is a PDF file of an unedited manuscript that has been accepted for publication. As a service to our customers we are providing this early version of the manuscript. The manuscript will undergo copyediting, typesetting, and review of the resulting proof before it is published in its final form. Please note that during the production process errors may be discovered which could affect the content, and all legal disclaimers that apply to the journal pertain.



**CARBON NANOFIBERS ENHANCE THE FRACTURE TOUGHNESS AND
FATIGUE PERFORMANCE OF A STRUCTURAL EPOXY SYSTEM**

Daniel R. Bortz^a, César Merino^b, Ignacio Martin-Gullon^{a,*}

^a*Department of Chemical Engineering, University of Alicante, Alicante, Spain*

^b*Grupo Antolín Ingeniería, Burgos, Spain*

Key Words: A. Nano composites, A. Carbon nanotubes, A. Polymer matrix composites (PMCs), B. Fatigue, B. Fracture toughness

Abstract

This study investigates the monotonic and dynamic fracture characteristics of a discontinuous fiber reinforced polymer matrix. Specifically, small amounts (0-1 wt%) of a helical-ribbon carbon nanofiber (CNF) were added to an amine cured epoxy system. The resulting nanocomposites were tested to failure in two modes of testing; Mode I fracture toughness and constant amplitude of stress tension-tension fatigue. Fracture toughness testing revealed that adding 0.5 and 1.0 wt% CNFs to the epoxy matrix enhanced the resistance to fracture by 66 and 78%, respectively. Fatigue testing at 20 MPa peak stress showed a median increase in fatigue life of 180 and 365% over the control by the addition of 0.5 and 1.0 wt% CNF, respectively. These results clearly demonstrate the addition of small weight fractions of CNFs to significantly enhance the monotonic fracture behavior and long-term fatigue performance of this polymer. A discussion is presented linking the two behaviors indicating their interdependence and reliance upon the stress intensity factor, K .

* Corresponding Author: Tel: +34 965903400 x2323; Email Address: gullon@ua.es (I. Martin-Gullon)

1. Introduction

Epoxy systems are widely used to bind laminates of glass or carbon fiber or to suspend particulate or fibrous fillers to create advanced multifunctional composite materials in which a high specific strength is required. Carbon nanomaterials offer remarkable properties and discontinuous carbon nanotube (CNT) and carbon nanofiber (CNF) reinforcement of epoxy matrices has shown potential to augment a variety of physical and mechanical properties resulting in truly multifunctional composite materials. Recent reviews by Spitalsky et al. [1] and Ma et al. [2] highlight the latest advancements. Understanding the monotonic and dynamic mechanical properties of structural epoxy reinforced with CNTs and CNFs will lend itself to the engineering of these advanced materials. In regard to the mechanical performance of these composites, interfacial adhesion between the matrix and reinforcing phase is essential [3, 4]. From a micromechanics of materials point of view, in which the matrix and reinforcing phase act as heterogeneous entities acting upon each other, shear stress build-up along the length of the interface is the mechanism responsible for stress transfer from the matrix to the fiber [5]. Inadequate fiber-matrix bonding is often cited as the explanation for unsatisfactory mechanical results.

When the stress intensity associated with an applied load exceeds the critical level needed to propagate a crack (K_{Ic}), energy is dissipated through fracture. Fracture toughness enhancements (and the mechanisms which govern them) through the addition of various micro and nano-sized particles in epoxy polymers are well cited in the literature [6-15]. Specifically, Gojny et al. [7] have demonstrated low concentrations of CNTs to increase the fracture resistance of an epoxy resin by approximately 25%. More recently, Palmeri et al. [15] have used the same CNF used in this work to demonstrate

fracture toughness enhancements of 45-80% in epoxy blends. Other work [10] though, has shown CNT reinforcement to negatively impact the fracture toughness of epoxy. It was shown that fracture resistance was only improved through surface functionalization with 3-glycidoxypropyltrimethoxysilane.

The fatigue failure of epoxy is the result of an initial reduction in stiffness due to the initiation of microscopic cracks at stress concentrating defects such as pores or material inhomogeneities. Repeated loading causes these cracks to grow and accumulate until ultimately, a runaway crack leads to rapid, catastrophic failure. The literature has indicated that the addition of rubber [16], metal [13], silica [17] and more recently CNTs [18-21] and graphene [12, 21] positively influence fatigue life and fatigue crack propagation rates when dispersed in epoxy matrices. Grimmer and Dharan [18] suggested that the addition of CNTs to a glass fiber epoxy composite resulted in the adsorption of strain energy through the creation of nanoscale cracks in tension-tension fatigue testing. It was observed that CNTs had a marked effect in high-cycle fatigue testing corresponding to low applied stress amplitudes. In this region, fatigue life was enhanced by 2.5 times over the non CNT-modified sample. Although the phenomena of crazing is not typically observed in epoxies due to its high crosslink density, Zhang et al. [20] provided SEM evidence of amido-amine-functionalized multiwall carbon nanotube (MWCNT) induced craze zones in fatigue crack propagation testing. It was argued that reinforcement was due in part, to the energy dissipative plastic deformation of the craze fibrils. In another report [22], the same group suggested that geometrical considerations and quality of dispersion are directly linked to fatigue improvements in MWCNT composite epoxy. It was maintained that reducing diameter, increasing length and

bettering the dispersion of MWCNTs significantly reduced the rate of fatigue crack propagation. Rotary bending fatigue tests at low stress magnitudes also suggested MWCNTs to improve fatigue life in epoxy [23]. Other reports have linked MWCNTs to significant increases in the fatigue life of thermoplastics such as PMMA [24-26]. To this regard, it was the aim of this study to test the effect of the addition of small amounts (≤ 1.0 wt%) of CNFs on the fracture resistance and fatigue performance of a structural epoxy system.

2. Experimental

2.1. Materials

Resoltech 1800/1805 (Resoltech, Eguilles, France), a low viscosity liquid epoxy system was used as the matrix. The epoxy resin, a reaction product of epichlorhydine with bisphenol A and bisphenol F, was cured with an amine hardener, 1,2-diaminocyclohexane. The mixing ratio was 100:17 parts by weight.

GANF, a commercial grade, helical-ribbon CNF was supplied by Grupo Antolín Ingeniería (Burgos, Spain) and used as provided [27-30]. GANF is synthesized by the continuous floating catalyst method using natural gas and sulfur as feedstock and a nickel compound as catalyst at approximately 1100 °C. The resulting CNFs are highly graphitic with no presence of an amorphous carbon coating. Outer diameters are heterogeneous, with an average of approximately 60 nm and a pre-processing aspect ratio (length/diameter) above 100. Structurally, GANF is comprised of a continuous graphitic ribbon helically rolled about the axis of the fiber (Fig. 1). Earlier TEM evidence [28] of unraveled fibers has confirmed their continuity and differentiates them from the discontinuous cones of the more common stacked-cup CNF morphology. Ribbons are

arranged $\sim 25^\circ$ oblique to the axis of the fiber and composed of approximately 5 individual layers of graphene [28, 31].

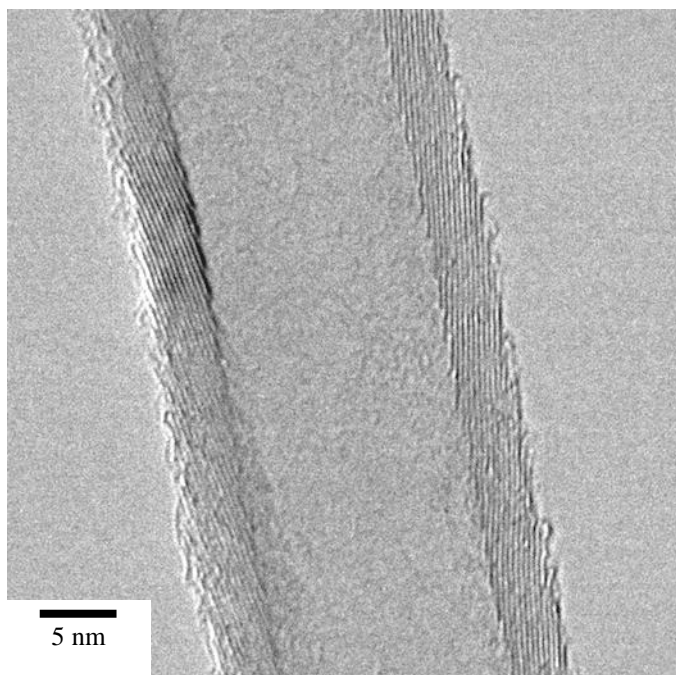


Fig. 1. A typical helical-ribbon carbon nanofiber viewed in high-resolution transmission electron microscopy. Note the ordered graphene layers oblique ($\sim 25^\circ$) to the axis of the fiber.

2.2. Sample preparation

After hand mixing, CNFs were dispersed in the epoxy resin using a high shear laboratory mixer (Silverson L4RT) at 7000 rpm for 15 minutes. The hardener was subsequently added and further mixed at 5000 rpm for 5 minutes. Dispersions were processed with 0.5 and 1.0 wt% CNF. A neat epoxy sample was similarly processed and used as a control. After mixing, the dispersions were poured into a silicone mold and degassed for 30 minutes at a vacuum approaching -1 bar. Individually cast test coupons, measuring $250 \times 25 \times 2.5$ mm for tension-tension fatigue testing, $63.5 \times 12.7 \times 4$ mm for Mode I fracture toughness testing and $30 \times 12.7 \times 3.2$ mm for DMA characterization,

were released from the mold after 12 hours at 40 °C. Additional heating in air for 15 hours at 60 °C and 6 hours at 110 °C completed the cure cycle. Specimen surfaces were smoothed on a rotary polishing machine using 320 grit followed by 600 grit silicone carbide grinding paper. Transmitted light (100×, Nikon Eclipse E200) and high-resolution transmission electron microscopy (TEM, JEOL 1020) verified dispersion. Testing was conducted 7 days after curing.

For fracture toughness testing, a 1 mm wide sharpened notch was machined at the mid-specimen point in the single edge notched bend (SENB) coupons. A pre-crack was subsequently introduced by tapping a fresh razor blade placed normal to the machined notch (Fig. 2). As per the standard, the ratio between the length of the notch plus the pre-crack (a) and the width (W) was between 0.45 and 0.55 for each specimen.

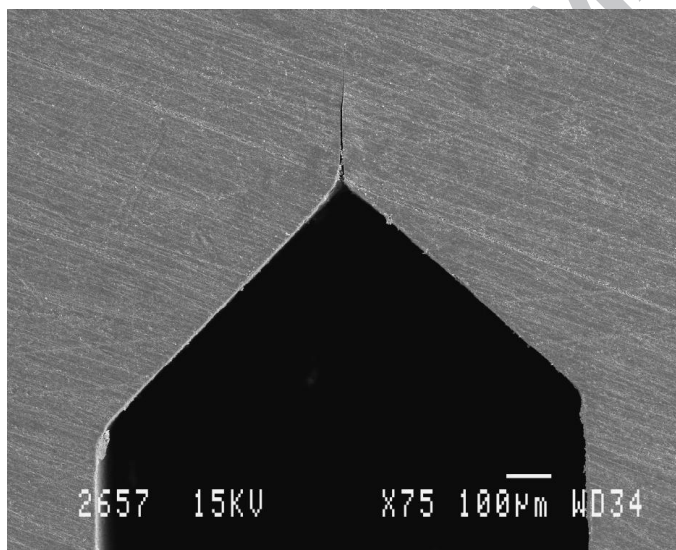


Fig. 2. Machined notch and pre-crack generated by tapping a fresh razor blade.

2.3. Dynamic mechanical analysis

Dynamic mechanical analysis (DMA) was performed in single cantilever mode using a TA Instruments 2980. Temperature ramps were carried out from 20 to 175 °C at a scan rate of 2 °C/min. The specimens were subjected to 20 µm amplitude of deflection at

1 Hz. This provided a strain of approximately 0.03% and was well within the linear elastic region. The glass transition temperature, T_g , was taken as the peak of the ratio of the storage modulus to the loss modulus ($\tan \delta$).

2.4. Fracture toughness testing

Mode I fracture toughness tests by the 3-point bending method (ASTM D 5045 [32]) were performed using an Instron 3344 (Instron Corporation, Canton, MA, U.S.A.) equipped with a 2 kN load cell. Three SENB specimens from each group were loaded to failure at a crosshead rate of 10 mm/min. Load-deformation curves were recorded and the pre-crack length was measured *post mortem* by optical microscopy. Testing was conducted at room temperature (25 °C). The critical-stress-intensity (K_{Ic}) needed to propagate the crack was calculated by

$$K_{Ic} = \left(\frac{P}{BW^{3/2}} \right) f(x), \quad (1)$$

where P is max applied load, B and W are specimen thickness and width and x is the ratio of the previously described crack length a and specimen width W . The function $f(x)$ is the second order polynomial found here [32]. The critical strain energy release rate (G_{Ic}) was computed by integration of the load-deformation curve used in the determination of K_{Ic} .

2.5. Fatigue testing and statistical analysis

Constant amplitude of stress tension-tension fatigue testing (ASTM D 3479M [33]) was performed at room temperature (25 °C) using an Instron 8516 100 kN servo-hydraulic materials testing system (Instron Corporation, Canton, MA, U.S.A.). No bonded tabs were used, instead an emery cloth interface functioned to prevent slippage and introduce the load to the specimen. Each test coupon was sinusoidally cycled between minimum and maximum in-plane axial load until failure at a frequency, $f = 5$

Hz. The ratio of the minimum to maximum applied load was $R = 0.1$. The number of cycles to failure (N) was recorded for each test coupon. Static tensile tests were carried out at a displacement rate of 2 mm/min using identical specimen geometry.

It was assumed that the fatigue life was normally distributed and the variance of $\log(N)$ was constant over the entire range of testing. In addition, the data contained no run-outs or suspended tests. Therefore, the cycles to failure were analyzed by constructing log-normally distributed $S-N$ curves transformed into linear form according to ASTM [34, 35] and expressed as

$$Y = A + BX, \quad (2)$$

where Y is equal to $\log(N)$, X is the maximum value of constant-amplitude cyclic stress and A and B are constants for each sample and estimated by

$$\hat{A} = \bar{Y} - \hat{B}\bar{X} \quad (3)$$

and

$$\hat{B} = \frac{\sum_{i=1}^k (X_i - \bar{X})(Y_i - \bar{Y})}{\sum_{i=1}^k (X_i - \bar{X})^2}. \quad (4)$$

Each test program involved two specimens tested at each of five stress amplitudes resulting in a replication of 50%. The variance in $\log(N)$ data was calculated by

$$\sigma^2 = \frac{\sum_{i=1}^k (Y_i - \hat{Y}_i)^2}{k-2}, \quad (5)$$

where \hat{Y}_i is the estimated fatigue life from the median $S-N$ curve from Eq. (2) and k is the total number of test specimens from each test program (in this case, $k = 10$). Hyperbolic

confidence bands taking into account all points on the median $S-N$ curve were computed using

$$\hat{A} + \hat{B}X \pm \sqrt{2F_p} \sigma \left[\frac{1}{k} + \frac{(X - \bar{X})^2}{\sum_{i=1}^k (X - \bar{X}_i)^2} \right]^{1/2}, \quad (6)$$

where $F_p = 4.4590$ and corresponds to $P = 95\%$. The confidence intervals are not designed to predict the inclusion of individual data points. Rather, it is expected that 95% of the computed hyperbolic confidence bands will include Eq. (2) over the entire range of X used in the testing program.

2.6. Scanning electron microscopy

Fracture surfaces from randomly selected failed specimens in both modes of testing were sectioned, sputter coated with gold and examined using high-resolution scanning electron microscopy (SEM, JEOL JSM-840). Qualitative conclusions were drawn from the micrographs on the fracture characteristics, reinforcement mechanisms and interactions between the CNFs and matrix.

3. Results and discussion

3.1. Dispersion of CNFs and degree of cure

A qualitative analysis indicated that the high-shear mixing protocol provided a respectable CNF dispersion throughout the epoxy matrix (Fig. 3). Though some agglomerations were observed, TEM exploration illustrated that the filaments were typically isolated and well wet by the matrix. Examination also revealed that the pre-processing aspect ratio of the CNFs was lessened to some extent. Filament shortening due

to high-shear mixing processes has been reported in other work and is often unavoidable in the dispersion process [36].

DMA results indicate no significant affect to the final degree of cure by CNF inclusion. The mean (standard deviation) T_g taken from the $\tan \delta$ peak for the neat, 0.5 and 1.0 wt% CNF materials were shown to be 126.3 (0.1), 126.9 (0.5) and 126.8 (0.3) °C, respectively. These values agree well with the manufacture's [37] figure of 130 °C for the given cure times and temperatures used here.

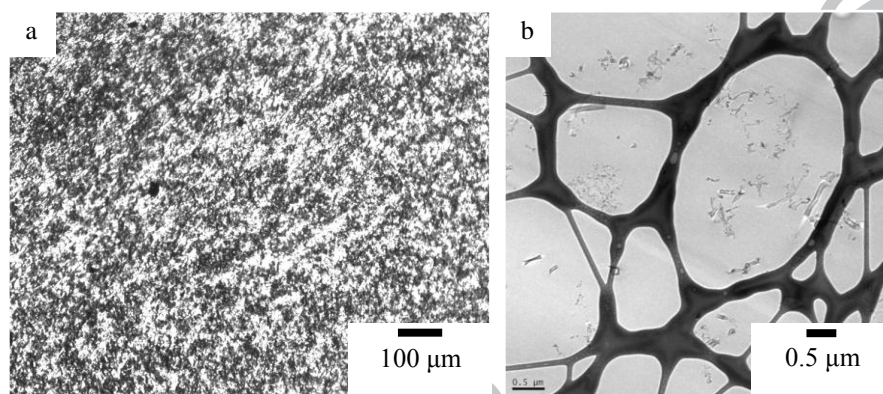


Fig. 3. (a) Transmitted light micrograph of 1.0 wt% CNF modified epoxy and (b) high-resolution TEM image of 1.0 wt% CNF/epoxy nanocomposite on a copper TEM grid.

3.2. Fracture toughness testing results

Results of fracture toughness testing for the neat epoxy matrix and two CNF composites (0.5 and 1.0 wt%) are shown in Fig. 4. Both toughness parameters indicative of resistance to fracture (K_{Ic}) and rate at which energy is absorbed by crack growth (G_{Ic}) were shown to significantly improve with increasing CNF concentration (Fig. 4a). The 1.0 wt% CNF loading resulted in the largest increase in K_{Ic} , i.e., from 0.74 MPa·m^{1/2} in the control group to 1.32 MPa·m^{1/2}, a 78% improvement. The corresponding enhancement in G_{Ic} over the neat sample at 1.0 wt% CNF was 144%. The 0.5 wt% CNF

loading resulted in smaller gains, yet the improvements in K_{Ic} and G_{Ic} were still 66 and 121% greater than the control group.

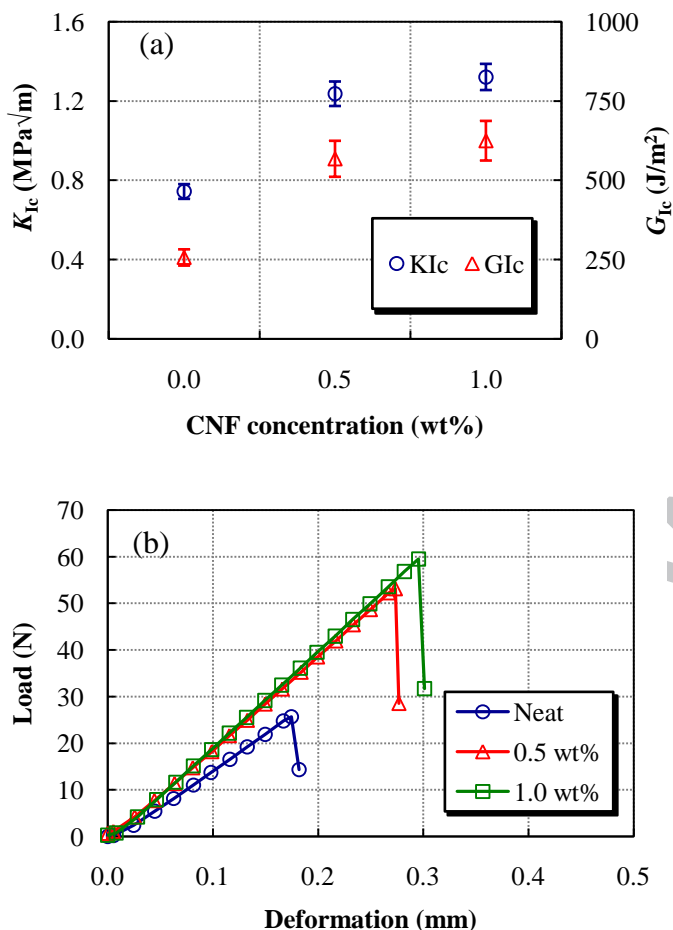


Fig. 4. (a) Mode I fracture toughness (K_{Ic}) and fracture energy (G_{Ic}) for neat, 0.5 and 1.0 wt% CNF modified epoxy groups and, (b) load-deformation curves of typical specimens from each sample.

Examination of fracture surfaces by SEM revealed the neat epoxy group to have the classic smooth fracture surface (Fig. 5a) observed in highly crosslinked polymer systems [38]. River marks leading to the initial site of crack growth were detected but substantial indications of plastic deformation in the control group were not noted.

Quantitatively speaking, the lack of observed plastic deformation and a smooth fracture

surface agree well with the relatively low measured toughness of the material ($K_{Ic} = 0.74 \text{ MPa} \cdot \text{m}^{1/2}$). Inspection of the 1.0 wt% CNF modified epoxy confirmed the group to display a much rougher fracture surface (Fig 5b). The formation of such additional surfaces during fracture is common to matrices reinforced with micrometer-sized particles and indicative of crack deflection [39].

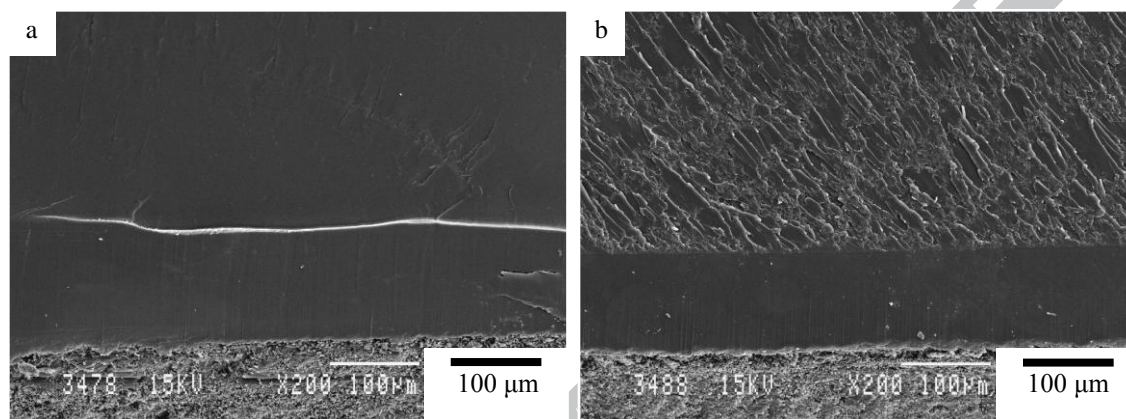


Fig. 5. Low-resolution SEM images of (a) a neat epoxy specimen illustrating the machined notch (bottom), pre-crack (middle) and mirror-like fracture surface (top) and (b) a 1.0 wt% CNF specimen exhibiting a rougher texture in the crack propagation zone. Crack growth is from bottom to top in both images.

3.3. Fatigue testing results

Raw loading and life data from the constant stress amplitude, tension-tension fatigue testing are listed in Table 1. Cyclic stress vs. lifetime ($S-N$) curves are shown in Fig. 6 and a summary of the log-normal fitting parameters is given in Table 2. Indicative of superior fatigue performance, the composites present much flatter $S-N$ curves and although fatigue life is augmented along the entire range of cyclic stress used in the testing, the addition of CNFs more significantly enhanced the fatigue life in the high-cycle, low-stress amplitude regime. Testing at the 20 MPa peak stress amplitude showed

the median fatigue life, as computed by Eq. (2), to increase by approximately 180 and 365% over the control with the addition of 0.5 and 1.0 wt% CNF respectively. The smallest improvement in median fatigue life was observed at the highest stress amplitude, 40 MPa. Here, a decrease of 15% in fatigue life was observed at 0.5 wt% CNF and an improvement of approximately 10% over the control was realized at 1.0 wt% CNF. Estimated variance in the log-normal distribution of each population was shown to be reasonably consistent across the control ($\hat{\sigma}^2 = 0.020$) and CNF modified samples ($\hat{\sigma}_{0.5 \text{ wt}\%}^2 = 0.035$ and $\hat{\sigma}_{1.0 \text{ wt}\%}^2 = 0.013$). Hyperbolic confidence bands corresponding to $P = 95\%$ were calculated by Eq. (6). Ultimately, these bands are expected to include the straight line from Eq. (2) 95 times out of 100. The inclusion of the confidence intervals illustrates the significance in the improvement of fatigue life at low applied stress amplitudes. At 20 MPa peak stress, the percent increase between the lower confidence band of the 1.0 wt% CNF modified epoxy and the upper band of the control still stands at approximately 105%. Beginning at approximately 33 MPa, the intervals overlap throughout the remainder of the higher applied peak stress amplitudes.

Table 1. Fatigue loading and life data for all test programs.

Table 1a Neat matrix		Table 1b 0.5 wt% CNF		Table 1c 1.0 wt% CNF	
N	σ_{\max} (MPa)	N	σ_{\max} (MPa)	N	σ_{\max} (MPa)
810	40.0	552	40.0	1 360	40.0
1 774	40.0	1 077	40.0	1 466	39.9
1 773	35.0	3 713	35.0	3 976	35.0
3 272	35.0	7 233	35.0	4 830	34.9
7 891	30.1	6 745	30.0	9 596	30.0
12 141	30.0	15 553	29.9	27 821	29.9
16 921	25.0	30 054	24.9	53 028	25.0
17 455	25.2	35 248	24.9	65 001	25.0
44 567	20.0	117 248	20.0	217 943	20.0
46 724	20.0	178 170	19.9	253 109	20.0

Table 2. Fatigue mean fit parameters (log values given for A and B).

Material	A	B	Coefficient of determination, R^2	Estimated normal population variance, $\hat{\sigma}$
Neat matrix	6.285	-0.080	0.986	0.141
0.5 wt% CNF	7.247	-0.106	0.930	0.188
1.0 wt% CNF	7.579	-0.112	0.983	0.114

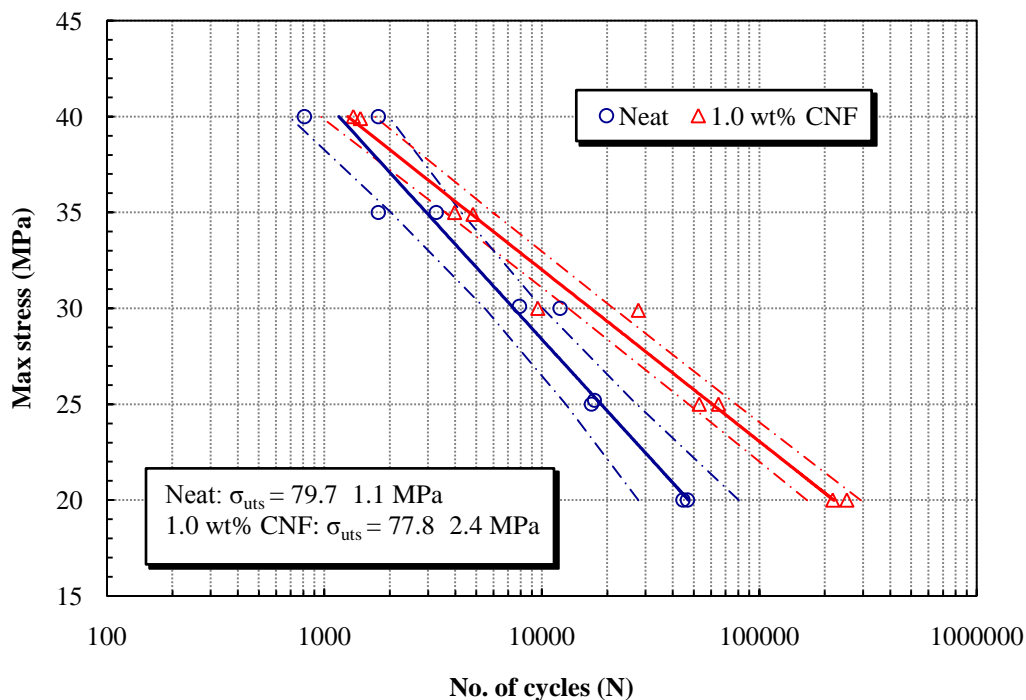


Fig. 6. Cyclic stress versus logarithmic scale of cycles to failure (S - N curves) for neat and 1.0 wt% CNF reinforced epoxy. Results from the 0.5 wt% CNF loading were between the neat and 1.0 wt% data but were omitted to avoid confusion. Hyperbolic confidence bands are as computed by Eq. (6).

Examination of fracture surfaces by SEM echoed the observations made from the fracture toughness specimens. A smooth, glasslike surface devoid of observable signs of plastic deformation was detected in the neat sample (Fig. 7a). River marks immediately surrounding and tracing back to the crack initiation site were common. The CNF

reinforced groups presented many more irregularities in their fracture surfaces. The jagged, multi-plane features observed in the 1.0 wt% CNF sample (Fig. 7b) appear to be evidence of the crack front being deflected and changing orientation during growth.

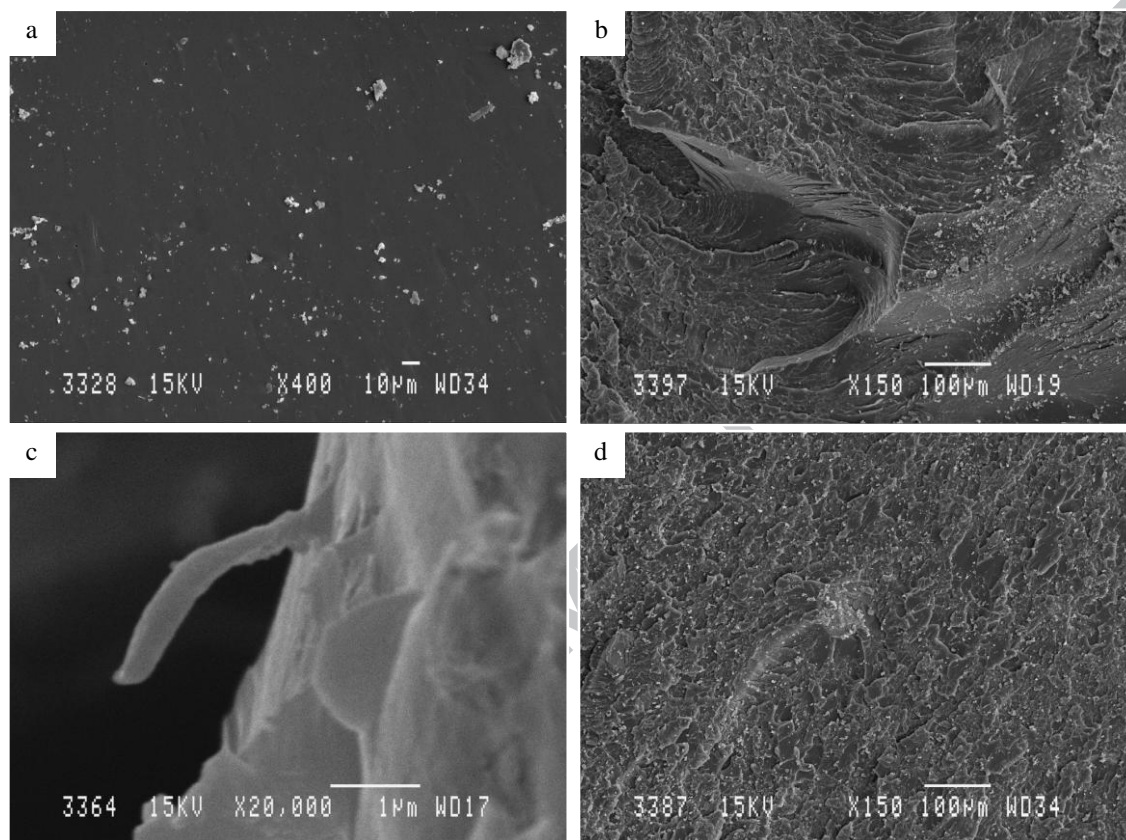


Fig. 7. A series of SEM images documenting (a) the typically smooth fracture surface of a neat specimen, (b) rough, multi-plane surface of a 1.0 wt% CNF loaded specimen, (c) a large diameter, isolated CNF protruding from the surface of a crack in a specimen stressed to 25 MPa and, (d) a CNF agglomerate. Crack propagation is from top to bottom in all images.

3.4. Toughening mechanisms

The quantitative K_{Ic} and G_{Ic} data presented here clearly show CNFs to enhance the fracture toughness of epoxy. Well-documented claims regarding the mechanisms for fracture energy dissipation in particulate reinforced thermosetting polymers include crack

pinning [13, 40-43], pullout and void nucleation [38, 44, 45] and crack deflection [46, 47]. Crack pinning has by and large been dismissed as an operating toughening mechanism in nanocomposites due to the matter of size compatibility [8]. Typical crack tip radii are dimensionally much larger than the nanometer-sized reinforcing phase. Nevertheless, reports of such occurrences have surfaced [13]. Fiber pullout, resulting from de-bonding of the fiber from the matrix causes fibers to bridge cracks in the wake zone behind the advancing crack tip. This mechanism has been characterized as the predominate mode of “overload failure” in fibrous nanocomposites [26]. The phenomenon, illustrated in Fig. 7c, is to be expected owing to the fact that the interfacial shear strength between the matrix and fiber has been shown to be less than the tensile strength of the fiber [48]. In some instances, crack bridging has been cited a dominant toughening channel [21]. In other reports though, it has been modeled to provide little overall reinforcement value [6]. Faber and Evans [46, 47] concluded that if the plane of a propagating crack could be altered in three dimensional space by the inclusion of a reinforcing particulate then a mixed-mode loading condition could result. The continual twisting and turning action of the crack front during fracture leads to mixed-Mode I, II and III loading and results in an increase in total fracture surface area (Fig. 7b). The energy absorbed by the creation of additional fracture surface area necessitates additional energy to be input to the system to continually drive crack growth (i.e., higher G_{Ic} values) [38, 46, 47]. The qualitative observation of increased fracture surface area and quantitative increase in G_{Ic} in this study appear to agree with the crack deflection theory proposed by Faber and Evans. Despite the inherent interdependence of the toughening mechanisms described above, it appears that the role of CNFs during crack propagation

are to aid in deflecting the advancing crack and force growth to deviate from the existing fracture plane.

Palmeri et al. [15] have reported a potentially new type of toughening mechanism for this variety of CNF. It was claimed, via supporting SEM and TEM evidence, that through the severing of the graphitic π - π interactions of the oblique graphene layers the fibers can either “discretely splay” or “continuously unravel.” The authors maintained the sacrificial bonding during unraveling could then lead to the fiber’s spanning of cracks and ultimately result in an increase in toughness. It is interesting to note the ability of the fiber to unravel its graphene layers has been previously demonstrated, albeit not in a composite [28]. The present study can neither confirm nor deny the phenomena’s manifestation in the matrix.

3.5. Effect of stress intensity and agglomerations

Results from fatigue testing indicate substantial and significant enhancement to the fatigue life of epoxy by the inclusion of a CNF reinforcing phase. Despite the reported positive effects of CNF addition in the high-cycle, low-stress amplitude fatigue testing regime, results from high-stress amplitudes (30-40 MPa peak stress) showed less than ideal results. The nonuniformity of the fatigue life increase at high applied stress levels is believed to be the result of two effects: (1) breakdown of the CNF/matrix interface and (2) CNF agglomerations (Fig. 7d) detracting from the positive reinforcing effect of individually dispersed fibers. Both conditions have a significant dependence on the stress intensity factor, K . At low applied stress levels, the interfacial strength of the CNF/matrix bond is believed to dominate localized stresses surrounding the crack tip. These stresses are effectively transferred from the weaker matrix and distributed in the

form of small-scale straining of the stiffer CNFs, preserving the elastic deformation of the bulk composite. This enables the fibers to actively interface with the matrix, shielding it from the buildup of stress and slowing the rate of fatigue crack propagation. Other studies have shown a strong dependence of stress intensity range (ΔK) in fatigue crack propagation rate testing [19, 21, 49]. An order of magnitude reduction in fatigue crack growth rate was observed at low applied ΔK with the addition of 0.5 wt% MWCNTs to an epoxy matrix [19]. At much higher ΔK values, a growth rate nearly identical to the neat matrix was evident. In this instance, the stress intensity surrounding the crack tip causes the CNF/matrix interface to break down. Ensuing crack propagation is ultimately the result of the localized stress intensity reaching the critical state, K_c . Thus, at smaller K values the CNFs more readily accept the transfer of stress. As K increases, the probability of crack growth due to interfacial failure heightens. For example, if we assume a fatigue crack has been naturally initiated at a single edge of a test coupon through repeated cycling, the Mode I stress intensity at the crack tip is given as

$$K_I = \sigma \sqrt{\pi a} F\left(\frac{a}{W}\right), \quad (7)$$

where σ is applied stress, a is crack length and W is coupon width [50]. Using Eq. (7) and assuming a reasonable crack length, a table containing applied stresses and corresponding stress intensity factors can be constructed (Table 3). In this instance the stress intensity at the crack tip in the low applied stress regime is much less than the critical value needed to propagate a crack (as indicated in fracture toughness testing). Beginning at approximately 30 MPa and continuing into the higher applied stress levels, K becomes exceedingly greater than the measured critical value. This example suggests that once a fatigue crack initiates in high stress amplitude fatigue testing, little can be done to delay

crack growth on the account of K being much higher than the measured critical value.

Here, catastrophic failure immediately follows crack initiation. Conversely, it is suspected that the CNFs play a greater role in the suppression of fatigue related damage in lower applied stress regimes.

Table 3. Maximum cyclic stress and corresponding Mode I stress intensity at the crack tip, as computed by Eq. (7). A crack length of 500 μm was assumed for this example.

σ_{max} (MPa)	K_I (MPa $\cdot\text{m}^{1/2}$)
10	0.45
20	0.89
30	1.34
40	1.79
50	2.23

4. Conclusions

The addition of helical-ribbon carbon nanofibers has been shown to significantly improve the fracture resistance and fatigue performance of a thermosetting epoxy system. The present results suggest that the influence of CNFs and their underlying mechanism of reinforcement are strongly K -dependent. In low applied stress amplitude fatigue testing, strain energy is interfacially transferred to the stronger CNFs due to the dominance of the interfacial strength over localized stresses. In high-stress amplitude fatigue and fracture toughness testing, interfacial strength is considered to be much less than the local stresses induced by increasing K near the crack tip. In this higher stress regime it is suspected that the CNFs function mainly to deflect propagating cracks. When the strain energy associated with loading overpowers interfacial strength, cracks form and propagate along the interface. The de-bonding action dissipates energy and ultimately incites deflection of the crack front. Ensuing mixed-mode loading (Modes I, II and III) from the deflecting

crack results in the observed increase in fracture surface area. Ultimately, the energy absorbed through these actions detracts from the available energy needed for crack growth. Together, these mechanisms lead to the enhancements in critical-stress-intensity factor and the energy per unit area of crack surface at the initiation of fracture. However, the expectation of reinforcement at stress intensities beyond K_{Ic} , as hypothesized to exist just after crack initiation in high-stress amplitude fatigue testing, is futile. Future work should examine more dispersive methods of incorporating CNFs to the matrix since the tendency of agglomerates in the high-applied stress regime is to incite crack initiation and accelerate propagation rates.

To summarize, the current results indicate the reinforcement of a structural epoxy system with CNFs has markedly heightened the materials resistance to fracture and significantly increased fatigue performance. Additionally, it has been shown that these conditions are strongly contingent on stress intensity.

Acknowledgments

Financial support for this work was provided in part by the Investigación en Nuevos Materiales para su Aplicación en la Industria Aeronáutica (NACAR) project through Grupo Antolín Ingeniería. We also thank Dr. Byung Chul Kim at the Korea Advanced Institute of Science and Technology for valuable discussions regarding fracture toughness testing.

References

- [1] Spitalsky Z, Tasis D, Papagelis K, Galiotis C. Carbon nanotube-polymer composites: Chemistry, processing, mechanical and electrical properties. *Progress in Polymer Science*. 2010;35(3):357-401.
- [2] Ma P, Siddiqui N, Marom G, Kim J. Dispersion and functionalization of carbon nanotubes for polymer-based nanocomposites: A review. *Composites Part A: Applied Science and Manufacturing*. 2010;41(10):1345-1367.

- [3] Bai J. Evidence of the reinforcement role of chemical vapour deposition multi-walled carbon nanotubes in a polymer matrix. *Carbon*. 2003;41(6):1325-1328.
- [4] Weisenberger M, Grulke E, Jacques D, Rantell T, Andrews R. Enhanced mechanical properties of polyacrylonitrile/multiwall carbon nanotube composite fibers. *Journal of nanoscience and nanotechnology*. 2003;3(6):535-539.
- [5] Jones R. *Mechanics of composite materials*: CRC; 1999.
- [6] Fiedler B, Gojny F, Wichmann M, Nolte M, Schulte K. Fundamental aspects of nano-reinforced composites. *Compos Sci Technol*. 2006;66(16):3115-3125.
- [7] Gojny F, Wichmann M, Köpke U, Fiedler B, Schulte K. Carbon nanotube-reinforced epoxy-composites: Enhanced stiffness and fracture toughness at low nanotube content. *Compos Sci Technol*. 2004;64(15):2363-2371.
- [8] Johnsen B, Kinloch A, Mohammed R, Taylor A, Sprenger S. Toughening mechanisms of nanoparticle-modified epoxy polymers. *Polym*. 2007;48(2):530-541.
- [9] Kim B, Park S, Lee D. Fracture toughness of the nano-particle reinforced epoxy composite. *Composite Structures*. 2008;86(1-3):69-77.
- [10] Ma P, Kim J, Tang B. Effects of silane functionalization on the properties of carbon nanotube/epoxy nanocomposites. *Compos Sci Technol*. 2007;67(14):2965-2972.
- [11] Nakamura Y, Yamaguchi M, Okubo M, Matsumoto T. Effect of particle size on the fracture toughness of epoxy resin filled with spherical silica. *Polym*. 1992;33(16):3415-3426.
- [12] Rafiee M, Rafiee J, Srivastava I, Wang Z, Song H, Yu Z, et al. Fracture and fatigue in graphene nanocomposites. *Small*. 2009;6(2):179-183.
- [13] Wetzel B, Rosso P, Hauptert F, Friedrich K. Epoxy nanocomposites-fracture and toughening mechanisms. *Engineering fracture mechanics*. 2006;73(16):2375-2398.
- [14] Zunjarrao S, Singh R. Characterization of the fracture behavior of epoxy reinforced with nanometer and micrometer sized aluminum particles. *Compos Sci Technol*. 2006;66(13):2296-2305.
- [15] Palmeri M, Putz K, Brinson L. Sacrificial bonds in stacked-cup carbon nanofibers: Biomimetic toughening mechanisms for composite systems. *ACS Nano*. 2010;4(7):4256-4264.
- [16] Manjunatha C, Taylor A, Kinloch A, Sprenger S. The tensile fatigue behaviour of a GFRP composite with rubber particle modified epoxy matrix. *Journal of Reinforced Plastics and Composites*. 2009.
- [17] Manjunatha C, Taylor A, Kinloch A, Sprenger S. The tensile fatigue behaviour of a silica nanoparticle-modified glass fibre reinforced epoxy composite. *Compos Sci Technol*. 2010;70(1):193-199.
- [18] Grimmer C, Dharan C. High-cycle fatigue of hybrid carbon nanotube/glass fiber/polymer composites. *J Mater Sci*. 2008;43(13):4487-4492.
- [19] Zhang W, Picu RC, Koratkar N. Suppression of fatigue crack growth in carbon nanotube composites. *Appl Phys Lett*. 2007;91:193109.
- [20] Zhang W, Srivastava I, Zhu Y, Picu C, Koratkar N. Heterogeneity in epoxy nanocomposites initiates crazing: significant improvements in fatigue resistance and toughening. *Small*. 2009;5(12):1403-1407.
- [21] Rafiee M, Rafiee J, Wang Z, Song H, Yu Z, Koratkar N. Enhanced mechanical properties of nanocomposites at low graphene content. *ACS nano*. 2009;3(12):3884-3890.

- [22] Zhang W, Picu R, Koratkar N. The effect of carbon nanotube dimensions and dispersion on the fatigue behavior of epoxy nanocomposites. *Nanotechnol.* 2008;19:285709.
- [23] Yu N, Zhang Z, He S. Fracture toughness and fatigue life of MWCNT/epoxy composites. *Materials Science and Engineering: A.* 2008;494(1-2):380-384.
- [24] Bortz D, Weisenberger M, Marrs B, Andrews R. Fatigue performance of multiwall carbon nanotube composite PMMA and ABS. *ASME*; 2008.
- [25] Marrs B, Andrews R, Pienkowski D. Multiwall carbon nanotubes enhance the fatigue performance of physiologically maintained methyl methacrylate–styrene copolymer. *Carbon.* 2007;45(10):2098-2104.
- [26] Marrs B, Andrews R, Rantell T, Pienkowski D. Augmentation of acrylic bone cement with multiwall carbon nanotubes. *J Biomed Mater Res.* 2006;77(2):269.
- [27] Martin-Gullon I, Vera J, Conesa JA, González JL, Merino C. Differences between carbon nanofibers produced using Fe and Ni catalysts in a floating catalyst reactor. *Carbon.* 2006;44(8):1572-1580.
- [28] Vera-Agullo J, Varela-Rizo H, Conesa JA, Almansa C, Merino C, Martin-Gullon I. Evidence for growth mechanism and helix-spiral cone structure of stacked-cup carbon nanofibers. *Carbon.* 2007;45(14):2751-2758.
- [29] Vera-Agullo J, Varela-Rizo H, Font R, Conesa J, Martin-Gullon I. Analytical pyrolysis as a characterization technique for monitoring the production of carbon nanofilaments. *Journal of Analytical and Applied Pyrolysis.* 2007;79(1-2):484-489.
- [30] Weisenberger M, Martin-Gullon I, Vera-Agullo J, Varela-Rizo H, Merino C, Andrews R, et al. The effect of graphitization temperature on the structure of helical-ribbon carbon nanofibers. *Carbon.* 2009;47(9):2211-2218.
- [31] Varela-Rizo H, Rodriguez-Pastor I, Merino C, Martin-Gullon I. Highly crystalline graphene oxide nano-platelets produced from helical-ribbon carbon nanofibers. *Carbon.* 2010;48(12):3640-3643.
- [32] Standard test methods for plane-strain fracture toughness and strain energy release rate of plastic materials. *ASTM D 5045-99.*
- [33] Standard test method for tension-tension fatigue of polymer matrix composite materials. *ASTM D 3479-96.*
- [34] *ASTM manual on fitting straight lines, STP 313: ASTM International; 1962.*
- [35] Standard practice for statistical analysis of linear or linearized stress-life (S-N) and strain-life (ϵ -N) fatigue data. *ASTM E 739-91.*
- [36] Andrews R, Jacques D, Minot M, Rantell T. Fabrication of carbon multiwall nanotube/polymer composites by shear mixing. *Macromol Mater Eng.* 2002;287(6):395.
- [37] Resoltech 1800, Technical data sheet. 2009.
- [38] Kinloch A, Taylor A. The toughening of cyanate-ester polymers Part I Physical modification using particles, fibres and woven-mats. *J Mater Sci.* 2002;37(3):433-460.
- [39] Kinloch A, Taylor A. The mechanical properties and fracture behaviour of epoxy-inorganic micro- and nano-composites. *J Mater Sci.* 2006;41(11):3271-3297.
- [40] Kinloch A, Maxwell D, Young R. The fracture of hybrid-particulate composites. *J Mater Sci.* 1985;20(11):4169-4184.
- [41] Evans A. The strength of brittle materials containing second phase dispersions. *Philosophical Magazine.* 1972;26(6):1327-1344.

- [42] Green D, Nicholson P, Embury J. Fracture of a brittle particulate composite. *J Mater Sci.* 1979;14(6):1413-1420.
- [43] Lange F. The interaction of a crack front with a second-phase dispersion. *Philosophical Magazine.* 1970;22(179):983-992.
- [44] Kawaguchi T, Pearson R. The effect of particle-matrix adhesion on the mechanical behavior of glass filled epoxies. Part 2. A study on fracture toughness. *Polym.* 2003;44(15):4239-4247.
- [45] Lee J, Yee A. Fracture of glass bead/epoxy composites: on micro-mechanical deformations. *Polym.* 2000;41(23):8363-8373.
- [46] Faber K, Evans A. Crack deflection processes--I. Theory. *Acta Metallurgica.* 1983;31(4):565-576.
- [47] Faber K, Evans A. Crack deflection processes--II. Experiment. *Acta Metallurgica.* 1983;31(4):577-584.
- [48] Barber AH, Cohen SR, Wagner HD. Measurement of carbon nanotube-polymer interfacial strength. *Appl Phys Lett.* 2003;82:4140.
- [49] Marrs BH. Carbon nanotube augmentation of a bone cement polymer. University of Kentucky, Biomedical Engineering, 2007.
- [50] Tada H, Paris P, Irwin G. *The stress analysis of cracks handbook* 3rd ed. 2000.